Materials Horizons

Accepted Manuscript

This article can be cited before page numbers have been issued, to do this please use: C. F. Guimarães, L. Gasperini, R. S. Ribeiro, A. F. Carvalho, A. P. Marques and R. L. Reis, *Mater. Horiz.*, 2020, DOI: 10.1039/D0MH00818D.

ROYAL SOCIETY OF CHEMISTRY

rsc.li/materials-horizons

View Article Online
DOI: 10.1039/D0MH00818D

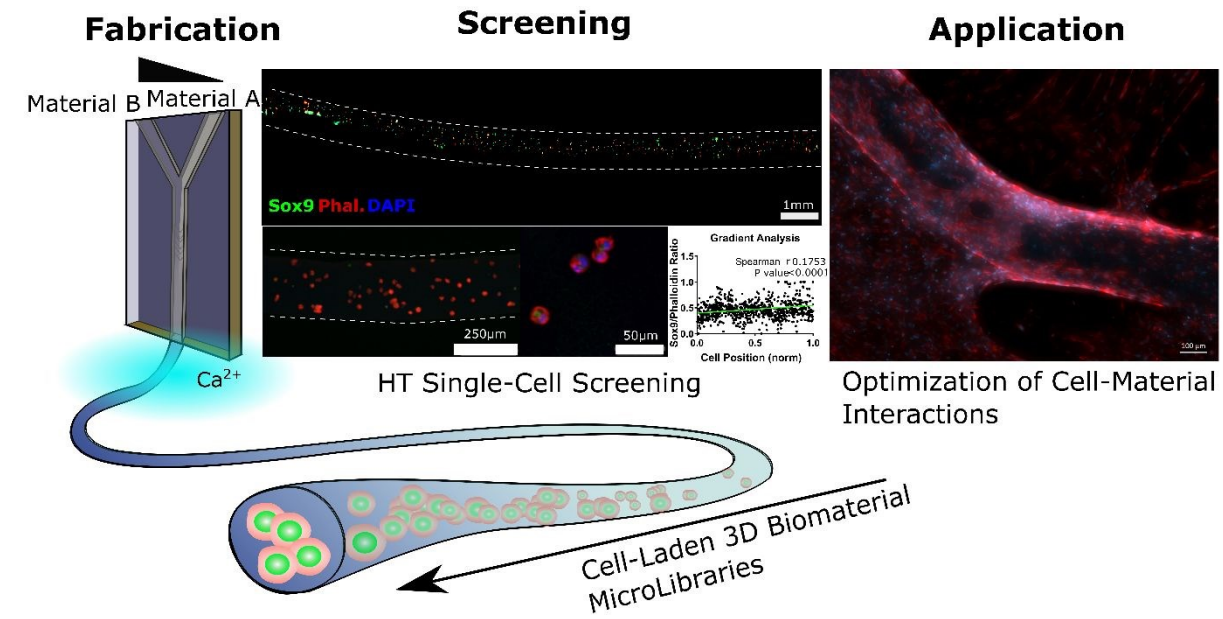

A fully high-throughput (HT) microfluidic platform for the generation of novel multi-material, multi-crosslinking 3D cell-laden gradients as screening libraries.

New concepts statement:

View Article Online
DOI: 10.1039/D0MH00818D

Current approaches to 3D biomaterial gradients as high-throughput (HT) screening platforms are mainly limited to light-based crosslinking as well as independent, single-gradient fabrication methods, therefore reducing the types of materials these can integrate as well as the desired HT of the whole approach.

We propose a simple and adaptable strategy wherein a custom microfluidic setup is employed to manipulate, mix and crosslink hydrogel precursors thus creating continuous structures with gradients in composition and overcoming current limitations. We show the possibility of fabricating gradients with a) ionic-crosslinking and UV-crosslinking materials; b) changes in the concentration of the crosslinking polymer and not only crosslinking time/exposure and c) including a full switch of both materials and crosslinking type within a single gradient.

We believe to be also first in simultaneously integrating 4 important premises of gradients as HT screening platforms: 1) quick and effortless production, reducing post-processing, 2) continuous analysis of single-cell responses along the gradient, 3) correlation between the response of cells and the material composition that elicits that response through microscopy-based analysis and 4) proven recapitulation of the screened cellular behavior in macro-sized, discrete hydrogels: the ones eventually applied for tissue engineering and regenerative medicine.

View Article Online
DOI: 10.1039/D0MH00818D

COMMUNICATION

High-Throughput Fabrication of Cell-Laden 3D Biomaterial Gradients

Received 00th January 20xx,
Accepted 00th January 20xx

DOI: 10.1039/x0xx00000x

Carlos F. Guimarães[1,2], Luca Gasperini[1,2], Raquel S. Ribeiro[1,2], Andreia F. Carvalho[1,2], Alexandra P. Marques[1,2] and Rui L. Reis[1,2,*]

High-throughput strategies for optimizing biomaterials to direct cellular behaviour are a fundamental need for propelling tissue engineering and regenerative medicine [1]. In 2D, biomaterial gradients have proven to be powerful platforms for simultaneously screening several surface conditions [2,3]. However, their translation to 3D is yet limited to 1) exploiting light-based crosslinking and 2) non-sequential, single-gradient production [4–6]. We built a microfluidic platform that allows distinct hydrogel precursors, as fluids, to be gradually mixed and crosslinked into 3D gradient fibres [7]. Herein, we report how this system can be used for the sequential fabrication of independent cell-laden libraries with gradients of polymer concentration, non-adhesive/adhesive materials and both ionic and light crosslinking mechanisms. Automated image analysis of hundreds of single-cell events as a function of position yielded trends and pinpointed best-fit conditions based on cell shape, adhesion, proliferation and triggering of stromal/stem cell differentiation. We deliver a simple, versatile, and complete approach towards fully high-throughput 3D gradient fabrication for cell/material screening and optimization.

The use of biomaterials for tissue engineering and regenerative medicine (TERM) is highly dependent on finding adequate formulations to support and direct cellular behaviour [1]. The low efficiency of the traditional, single-sample screening approach fails in a time where a vast number of available biomaterials can potentially be used for a specific application. This leads to a fundamental need for faster and reliable high-throughput (HT) screening technologies. True HT platforms, however, require that all stages have equally high efficiency, namely the fabrication of the libraries, the automated analysis, and the processing of the output data [8]. Across the literature, one can find two major types of HT platforms: (micro)arrays and gradients.

On the one hand, arrays or (more frequently) microarrays are the most obvious example of HT platforms, which consist mostly on the concentration of up to thousands of small spots of different biomaterials within a small surface [9]. These spots have variations in surface parameters such as chemistry and topography or, instead, distinct 3D droplet-like micro structures with different cell-laden materials [10].

Gradients, on the other hand, are a type of HT library where full ranges of the conditions of interest are integrated within a single sample, which changes gradually with space. Like arrays, gradients have been used for screening cellular responses to distinct biomaterial properties, such as surface stiffness [2] and topography [3] . In 3D hydrogels, gradients have also been fabricated to integrate ranges of different physical and biochemical cues [4,11,12]. Most of these are, however, manufactured using controlled light exposure and light-crosslinking materials [4,5,11,12], a limitation that prevents the study of e.g. ionic crosslinking materials.

Additionally, for gradients to live up to the HT challenge and be fair opponents of high-throughput arrays, we believe these should be capable of not only performing as well in terms of production and automatization but go a step further by exploiting continuity of analysis instead of discrete array-like screening. For this to happen, we believe gradients should adhere to four main premises, which are yet to be conjugated in a single approach: 1) Automatable and sequential production – gradient fabrication should be easily reproducible, preferably sequentially as time-consuming strategies compromise throughput; 2) Continuous analysis of cell responses as a whole and not limited to 3 or 4 gradient regions – this compresses the information present within the gradient and moves closer to a low-throughput strategy with discrete samples; 3) Connection between cellular response and material composition - suggesting that gradients should be kept intact throughout all screening stages so that cell responses can be associated to a gradient position, which can be associated to a specific formulation by knowing how the gradient is built, e.g., linearly changing compositions. This is the reason why microscopy and similar imaging approaches are the current best-in-slot techniques for gradient HT screening [2–6]. Finally, 4) cellular responses within the gradients must recapitulate those that take place in uniform, macro constructs: the ones which will eventually be used for TERM.

[1]3B's Research Group — Research Institute on Biomaterials, Biodegradables and Biomimetics, University of Minho, Headquarters of the European Institute of Excellence on Tissue Engineering and Regenerative Medicine, Guimarães, Portugal.
[2]Life and Health Sciences Research Institute, 3B's Research Group on Biomaterials, Biodegradables and Biomimetics – Portuguese Government Associate Laboratory, University of Minho, Braga and Guimarães, Portugal.

*e-mail: rgreis@i3bs.uminho.pt

Electronic Supplementary Information (ESI) available: [details of any supplementary information available should be included here]. See DOI: 10.1039/x0xx00000x

Herein, we report the generation of a HT platform for the screening of cell-biomaterial interactions that addresses all those needs. We started by exploring the potential of microfluidics for fabricating hydrogel libraries based only on ionic crosslinking materials, which form hydrogels under fast-yet-mild conditions and have seen continuously increasing value for TERM [13]. For this purpose we used Gellan Gum (GG), a common hydrogel that crosslinks in the presence of any cation such as Na+ and Ca^{2+} [14].

Hypothesizing that the concentration of GG and consequent hydrogel mechanics could impact the triggering of cell differentiation, we started our study on low-throughput macro-hydrogels with increasing gelling polymer concentration (**fig. 1a**) together with corresponding continuous microfluidic-generated 3D fibres (**fig. 1e**), which served as a framework for the validation of our high-throughput strategy. We established a concentration range of 0.5-1 w/vol% GG hydrogels, which led to a storage moduli interval of 5-20 kPa (**fig. 1b, i, S2**), close to those of several living tissues [15]. We then studied the effects of varying the concentration of GG in the behaviour of human adipose-derived stromal/stem cells (hASCs), which we used as a model primary cell type widely used in TERM [16]. To discard any negative effect of the encapsulation of these cells, their viability was assessed confirming 70-80% live cells throughout the first week of analysis (**S3**), in line with previous reports using the same material [17]. Within 3D environments, the mechanical properties of the encapsulating material can significantly impact the shape of cells as well as their commitment even if only through mechanical confinement which might be even more significant in non-adhesive environments [18,19]. Cell size and triggering of differentiation were then defined as the parameters to screen the effect of the mechanical environment provided by the different GG hydrogels. Image analysis of Calcein AM signal as an indicator of cell size revealed a decrease in projected cell area with increasing GG concentration and hydrogel stiffness (**fig. 1b, ii**), hinting at a mechanical restriction on cell expansion. Throughout this work, we used maximum projection images for analysis to condensate 3D information in 2D objects and allow for both faster full-structure imaging and automated image analysis, as described in the supplementary methods section. Even if some detail might be lost, 2D projections are still routinely used for efficiently analysing 3D structures in the HT scenario [20].

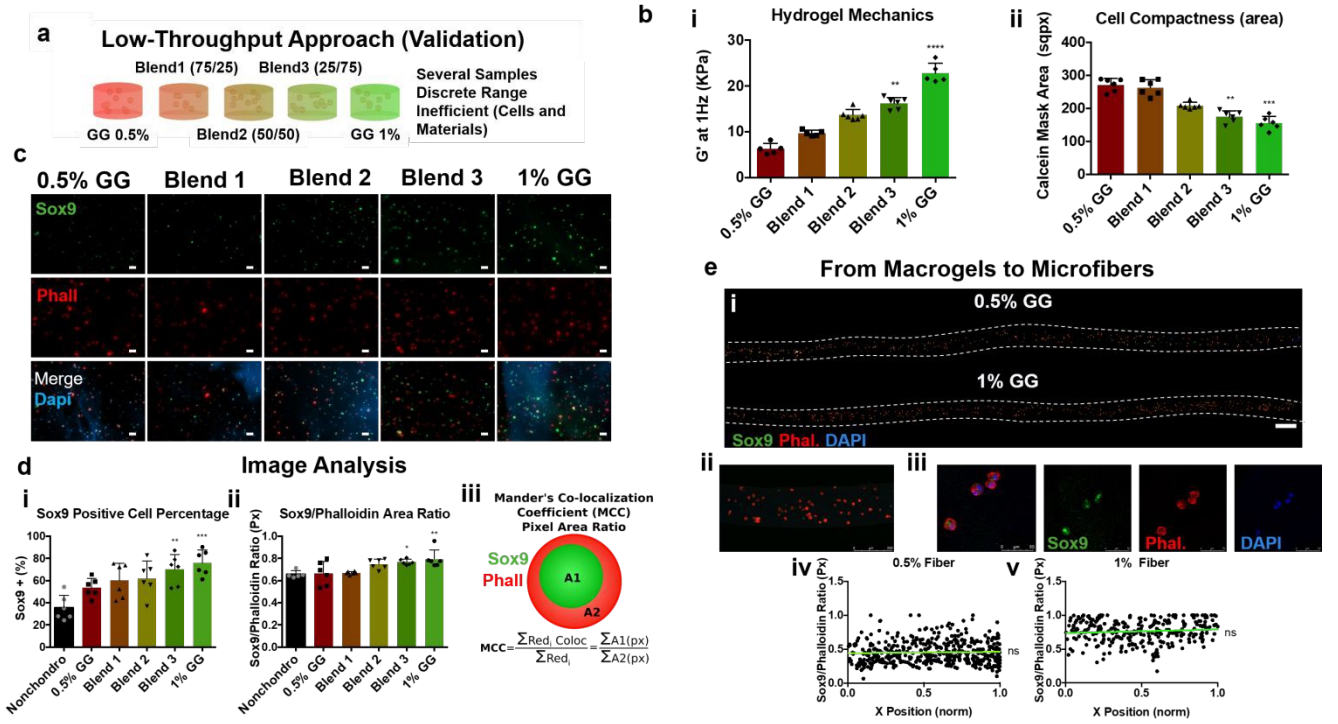

Fig. 1: Low-Throughput Hydrogels and Uniform Microfibres. a | Rationale behind a low-throughput biomaterial testing strategy where single-sample testing takes place over a discrete range of specific conditions. b | On uniform Gellan Gum (GG) macro-hydrogels (8mm disks), the mechanical analysis revealed a 5-20 kPa range from gradually blending 0.5% and 1% solutions of the polymer (i). Image analysis after Calcein AM staining shortly after encapsulation revealed decreasing projected cell areas in the higher concentration hydrogels, hinting at increasing cell compactness (ii, **S3**). Statistical values: ** p<0.01, *** p<0.001, compared to 0.5%GG. c | After 1 week in chondrogenic culture, significant changes could be observed in the expression of SOX9 by hASCs (Green, Scale bar 50µm). Cell nuclei were stained with DAPI (blue) and cytoskeleton actin with Rhodamine-labelled Phalloidin (Red). Slight blue background shades are visible due to a certain fluorescence of GG within the UV range. d | Using an image analysis pipeline, we could detect a significant increase in the percentage of SOX9+ cells (i) as well as in the SOX9/Phalloidin Pixel ratios (ii), which were obtained by taking advantage of Mander's Co-localization Coefficient and the particular signal co-localization that exists in encapsulated cells (iii). *Nonchondro*: no chondrogenic stimuli, NC. *Blend 1*: 75:25 Mixture of GG 0.5%:GG 1%; *Blend 2*: 50:50 Mixture of GG 0.5%:GG 1%; *Blend 3*: 25/75 Mixture of GG 0.5%:GG 1%. e | Cell-laden GG hydrogel microfibres of uniform composition (0.5% and 1%) were prepared by wet-spinning the material into a crosslinking bath (scale bar 500µm) via a linear microfluidic channel (i). Detailed confocal zoom-in into a specific gradient section (ii) and detail of single cells inside the hydrogel (iii) are imageable due to the low thickness and transparency of the fibres. hASCs-laden fibres were cultured and immunostained as described for the macro hydrogels. By performing image analysis, the behaviour of cells was tracked according to their X position along the fibres, revealing no significant trend within these uniform structures (iv, v).

View Article Online
DOI: 10.1039/D0MH00818D

When cultured in chondrogenic differentiation medium, hASCs expressed the master-regulator of chondrogenesis, SOX9 [21] (**fig. 1c**). Image analysis was used to quantify the percentage of SOX9 positive cells (**fig. 1d, i**) and the SOX9/Phalloidin total pixel (area) ratios (**fig 1d, ii**). This analysis revealed a significant increase of SOX9 expression (chondrogenic triggering) in the stiffer hydrogels by both metrics. To reduce acquisition-related variations, we opted by performing this analysis based on the signal area instead of intensity (**fig. 1d iii**). By performing a normalization of SOX9 area to Phalloidin area (total pixels), we compensated for visible variation in the 3D volume and respective 2D projected area of cells, which could have very different SOX9 areas but in the end similar when considering the total cell size. The image analysis approach was validated through western blot where protein levels reflected the same response and identified also Blend 3 (25:75 mixture of 0.5% and 1% GG, respectively) and 1% GG as the best conditions for triggering chondrogenic differentiation of hASCs (**S4**).

Once we understood the behaviour of cells on macro hydrogels and validated our analysis metrics, we moved towards the miniaturization of 3D environments by fabricating uniform hydrogel microfibres. Gellan Gum fibres were created by wet-spinning the hydrogel precursor into a crosslinking bath using a linear microfluidic channel (**Svideo**), creating continuous, linear hydrogels with encapsulated hASCs (**fig. 1e**, **i-iii**). In order to validate the hydrogel microfibres as suitable analysis platforms, the trend of SOX9 responses of individual cells were imaged and analysed (**S7**), as done for the macro hydrogels. In this case, the response of each individual cell was plotted according to its X position, obtaining a distance/response profile along the fibre. Herein, no significant changes in SOX9 responses were observed along the uniform environments, although responses in 1% GG fibres were comparably higher than those in 0.5% GG fibres (**fig. 1e iv, v**), which approaches what we observed in the previously discussed macro hydrogels. To move towards the fabrication of equivalent 3D gradient libraries **(fig 2a**), we connected the distinct material components to an herringbone mixing stage [22] prior to the output linear chip (**S5**) and gradually combined the flows of the 2 end-point materials (0.5% and 1% GG) (**fig. 2 b**), resulting in a balanced gradation in composition, where the whole range of GG concentration was combined into a single sample (**fig. 2c, i**). Therein, no presence of Janus-like separation between the two endpoint components was present, evidencing a successful disruption of purely laminar flows and consequent mixing of the precursors. As such, we obtained a gradient which was composed of purely ionic-crosslinking components, formed by gradual mixing and spinning, representing the first library of its kind. Once the gradient was successfully fabricated, we tested if cells could be manipulated and mixed together with the materials and observed no negative impact on their viability (**fig. 2c, ii, S6**).

It has been reported by other authors that softer environments favour adipogenic commitment [23,24] and stiffer ones promote higher levels of chondrogenic differentiation [25]. To verify if we could screen similar responses within GG hydrogels, we used our gradients to track the response of each encapsulated cell after 1 week of culture in either chondrogenic or adipogenic differentiation media, to look for the 3D environment which would better synergize with those distinct culture conditions and potentiate the triggering of differentiation. Plotting the expression of the respective master differentiation markers [21,26] as a function of distance, it was possible to observe that the

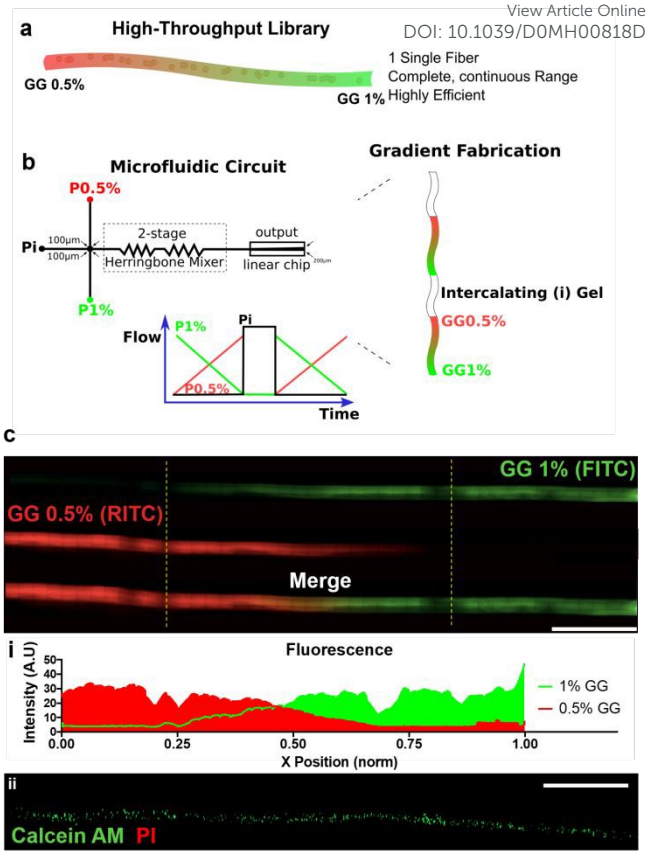

Fig. 2: Gellan Gum Gradients. a | Rationale of a gradient fibre as a high-throughput library, where a full range of conditions is integrated into a single sample as opposed to several discrete ones. b | To fabricate gradients, a microfluidic circuit was used to manipulate 2 endpoint materials through pressure regulation (P0.5%, P1%), gradually increasing/decreasing the first/latter flows, forcing the total flow through an herringbone mixer chip in order to ensure mixing of the hydrogel precursors [22]. By intercalating gradients with an empty material (PI), we were able to sequentially fabricate individual libraries. c | The gradient technique generates a fibre with a gradual change in composition (scale bars 0.5mm), which was followed by tracking RITC (red) and FITC (green) coloured GG (i). The encapsulation of cells and their microfluidic manipulation had no negative impact on hASC viability (live Calcein AM (Green) and dead Propidium Iodide (Red) cells) (ii).

triggering of chondrogenic differentiation (SOX9 expression) (**fig. 3a)** trended in a different direction than that of adipogenic commitment (PPAR-γ expression) (**fig. 3b)**. Based both on the SOX9/Phalloidin and PPAR-γ/Phalloidin pixel ratios (**fig. 3a, 3b ii**) as well as intensity (**fig. 3a, 3b iii**) of the signals, chondrogenic triggering increased significantly with GG concentration (**fig. 3a**) while adipogenic differentiation seemed to oppositely benefit slightly more from the softer environments (lower GG concentrations) (**fig. 3b**). The observed SOX9 expression reflected the ones observed in the low-throughput approach (**fig. 1**) for the chondrogenic differentiation. In regards to the PPAR-γ responses, the observed trend, overall slight yet detectable, also supports previous results concerning the adipogenic differentiation in soft GG hydrogels [27].

Therefore, by single-sample screening, we were able to quickly detect trends and identify the most appropriate formulations to trigger two distinct commitment pathways, both

View Article Online

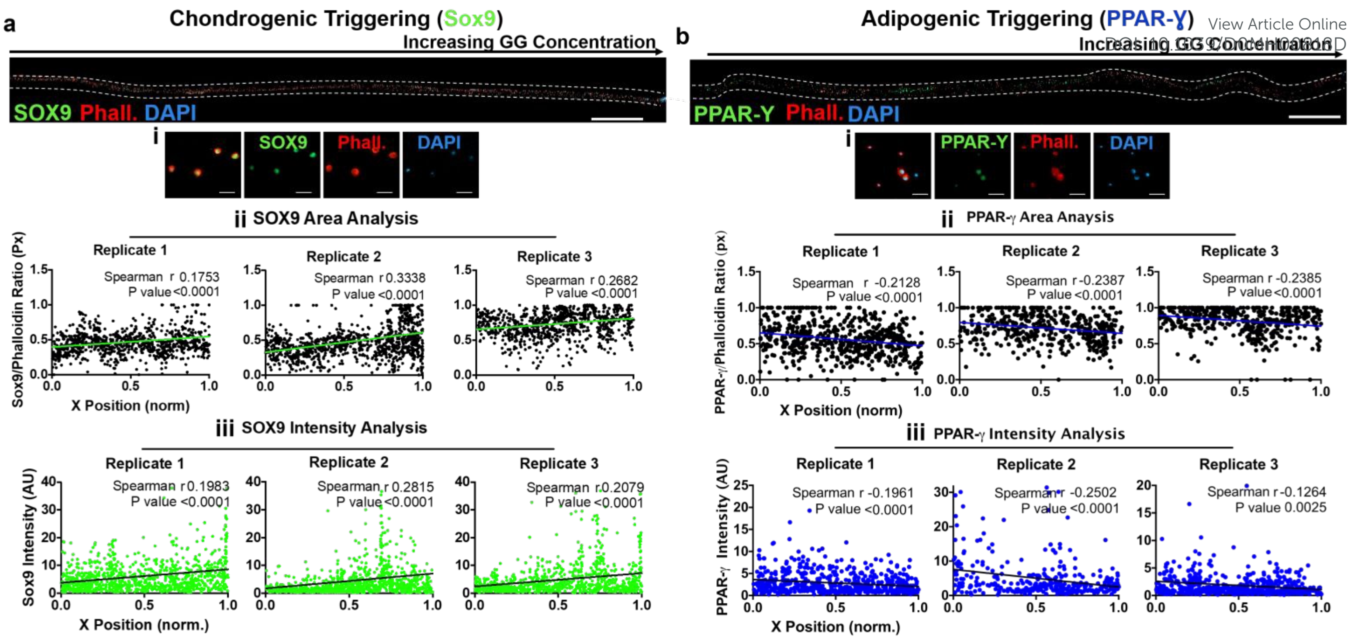

Fig. 3: hASC differentiation triggering in GG Gradients: a| Within the gradients, hASC responses were tracked upon 1 week of culture in chondrogenic conditions (full gradient scale bar 0.2mm, single cells representative marker detail (i) scale bar 50μm). Hundreds of single-cell responses evidenced a significant increase in the SOX9 levels along all 3 gradient replicates (each graph containing data from a single replicate) both considering SOX9 area (ii) and intensity (iii), pinpointing stiffer environments as better triggers of chondrogenic differentiation. b | After 1 week under adipogenic stimuli, it was possible to see that, oppositely to chondrogenic differentiation, the adipogenic triggering as shown by the expression of PPAR-γ (full gradient scale bar 0.2mm, single cells representative marker detail (i) scale bar 50μm) decreased along all 3 gradient replicates (each graph containing data from a single replicate) both considering area (ii) and intensity (iii) of the staining, placing softer environments as slightly better fit for adipogenic induction. Cell responses were evaluated after immunocytochemistry against SOX9 and PPAR-γ (green), cell nuclei counterstaining with DAPI (blue) and actin cytoskeleton with rhodamine-phalloidin (red). In all cases, r and p values correspond to the resulting Spearman correlation analysis.

mirroring the responses taking place at the molecular level on larger hydrogel structures.

Overall, the responses of cells encapsulated within non-adhesive environments such as pure GG are limited by the absence of direct cell-material interaction. Thus, in order to increase the complexity of our platform, going beyond extracellular mechanics and further screening cell adhesion-dependent responses - both properties that synergize in ECM-like environments [28] - we introduced an adhesive component, Gelatin Methacryloyl (GelMA), capable of direct cell-material interaction.

As we combined the mostly-bioinert GG with the much more biolabile GelMA [29] (**fig 4a**) we could observe the formation of stable hydrogels with physiological-range [15] mechanics (**fig 4b**). We then adapted our platform to operate at 37ºC (**S8**), allowing the production of gradients with a transition from GG to GelMA by gradually decreasing the first and increasing the latter (**fig. 4c**).

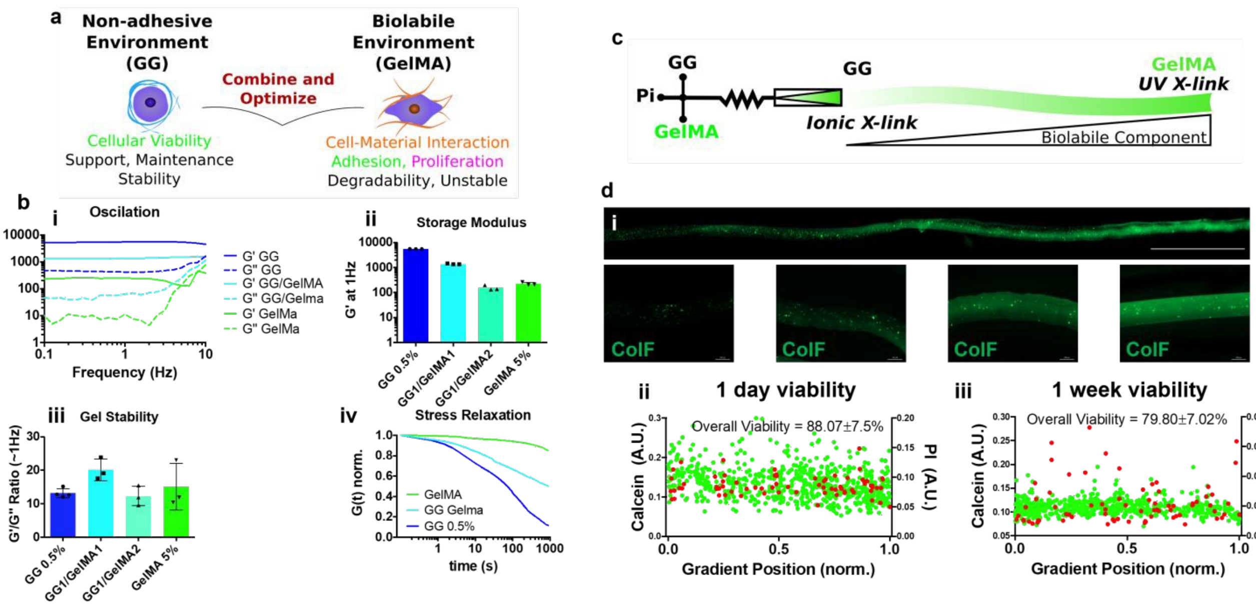

View Article Online
DOI: 10.1039/D0MH00819D

Fig. 4: Inert/Adhesive Gellan Gum-Gelatin Gradients. a | GG and GelMA were considered as materials capable of supporting respectively non-adhesive and more biolabile environments for cells. b | Both materials were mixed and dually crosslinked forming hydrogels with physiological-range mechanics (i,ii) and stable structures (G'/G'' ratios above 10) (iii). Stress-relaxation analysis also revealed an intermediate GG/GelMA behaviour between the stress-relaxing GG (ionic) and the non-relaxing GelMA (covalent) (iv). GG1/GelMA1 – 1:1 Blend of GG:GelMa, GG1/GelMA2 – 1:2 Blend of GG:GelMa. c | Schematics of the fabrication of the GG-GelMA gradients with our microfluidic system. d | Gradients were confirmed after staining the cell-laden structures with ColF (green, scale bar 0.5mm). Within the gradients, the proportion of viable (Calcein-positive cells in green dots, PI-positive cells in red dots) was maintained regardless of the local gradient composition and crosslinking both after 1 day (ii) and 1 week (iii) of culture.

This gradient, where a gradual increase in GelMA was confirmed by the specific ColF staining [30] (**fig. 4d, i, S9**), represents two important advances. On one hand, it is a multi-material gradient integrating a full switch in composition rather than modifications of a same hydrogel as approached in previous works [4,11,12]. On the other hand, this change in materials is further combined with a shift in the crosslinking strategy, from the ionic-crosslinking GG to UV crosslinking GelMA, which also represents an important advance in gradient complexity. Nevertheless, regardless of the type of material or crosslinking used to produce the gradients, the proportion of viable cells was not visibly affected (**fig. 4d ii, iii, S10**).

In order to assess the applicability of these inert/adhesive gradients as platforms in which cell adhesion and consequent responses to different materials could be screened, we looked at cellular morphology and adhesion, as well as mechanotransduction and proliferation responses. Changes in cell morphology and adhesion upon 1 week of culture within the GG/GelMA gradients were assessed based on cell cytoskeleton-related parameters (cell shape and form factor) and on the overall expression of the adhesion protein Paxillin (**fig. 5a**). From the image analysis, a significant increase in cell area (**fig. 5a, iv**) and decrease in form factor (**fig. 5a, v**), evidence of larger, less round cells - hinting at increasing cell-material interaction - was detected for increasing GelMA amounts. Simultaneously, Paxillin intensity per cell increased along the gradient with the increasing GelMA amounts, evidencing a higher degree of cell adhesion (**fig. 5a, vi**). Curiously, we noticed not only a trend but also a specific region - within the gradients and among replicates - where both cell area and paxillin intensity trends appeared to shift from constant to successively increasing with GelMA amounts. This happened at around half of the gradient position (arrows in **fig. 5a iv** and **vi, S11, S12**), which corresponds to approximately 1:1 GG/GelMA ratio, as the gradient was built linearly (**fig. 2b, S9**).

We further looked at markers of cell proliferation and mechanotransduction by quantifying the expression of Ki-67 and YAP, respectively (**fig. 5b**). Overall, the recreated environments did not seem to extensively favour the proliferative state of the cells upon 1 week of culture, as only a few cells were Ki-67 positive (**fig 5b, iv**). Nevertheless, most of these were present in the second half of the gradient, i.e., after the 1:1 GG/GelMA threshold (**fig 5b, iv, S13**). Interestingly, YAP intensities significantly increased along the gradient, also with an apparent shift present in some gradients around the 0.5 position (normalized) of the fibres (**fig 5b v, S14**). Nevertheless, no significant changes in the nuclear/cytoplasmic YAP ratios were detected (**fig 5b vi, S14**). Even if the increasing cell-material interaction leads to higher YAP expression, there appear to be no detectable differences in its nuclear shuttling. This suggests no specific YAP-dependent differentiation pathways were changing [31] under the gradient culture conditions. In fact, it was previously shown that YAP-related mechanotransduction might not be so impactful in soft 3D environments as it is in 2D scenarios [32].

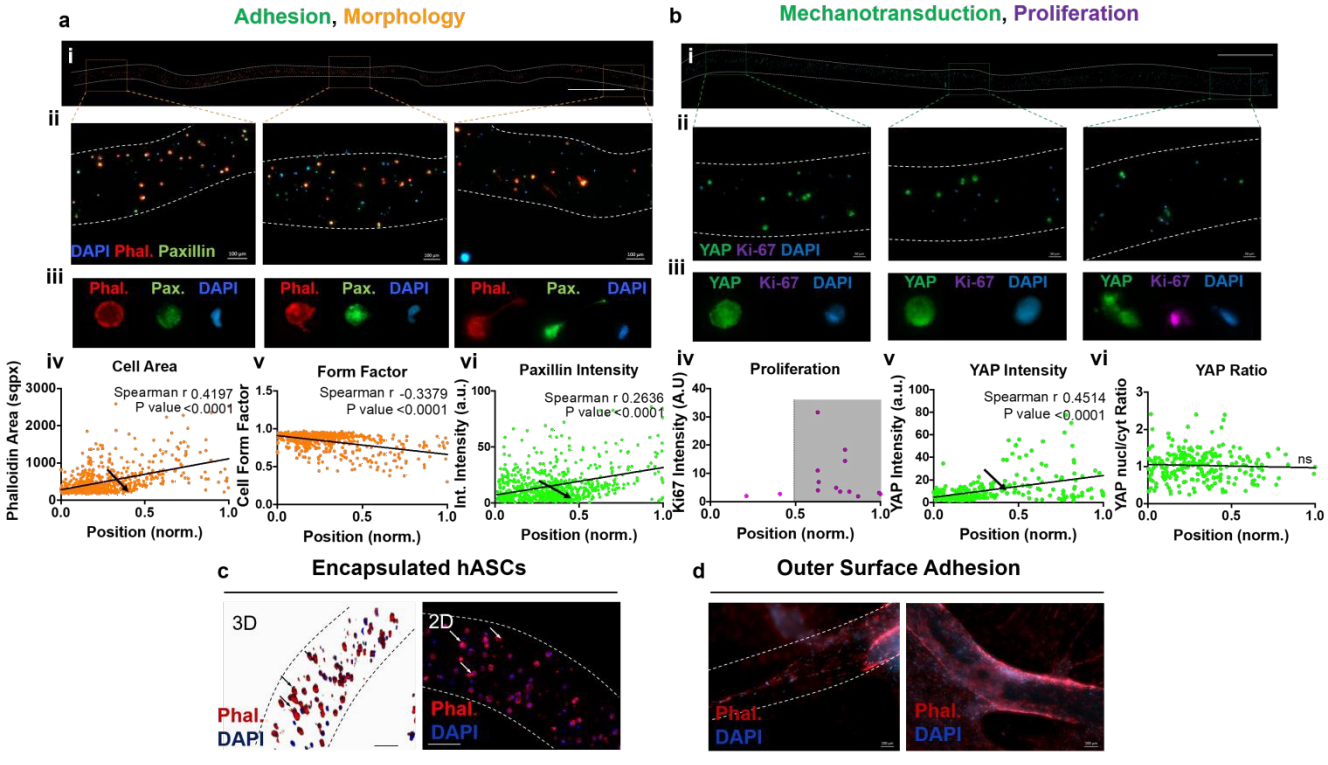

View Article Online
DOI: 10.1039/D0MH00818D

Fig. 5: hASC Responses in GG-GelMa Gradients. a | hASC adhesion and morphology was tracked by Phalloidin (red) / Paxillin (green) / DAPI (blue) staining (i, scale bar 5000µm, ii, scale bar 100µm) upon 1 week of culture within GG-GelMA gradients. Single-cell representative images of 3 gradient regions (start, middle, end of the fibre) are also shown (iii). Representation of Cell Area (iv) and Form Factor (v) (phalloidin-based image analysis), and Paxillin intensity as a function of gradient distance (increasing GelMA-to-GG) (vi). Black arrows point to the half region of the gradient, where a shift in cell responses can be observed. b | Proliferation (Ki67, purple)- and mechanotransduction (YAP, green)-related markers' expression was also assessed (i, scale bar 5000µm, ii scale bar 50µm, iii representative single cells); Ki67+ cells (purple dots) were overall rare and mostly only detected after half of the gradient (1:1 GG:GelMA ratio) towards increasing GelMA amounts (iv). YAP intensities significantly increased along the gradient (v), also evidencing a slight shift around the 0.5 position (normalized) (black arrow). No significant differences were detected in the nuclear/cytoplasmic YAP ratios (vi). All graphics are representative of the gradient replicates found in supplementary data. c | Uniform hASC-laden fibres fabricated with 1:1 GG/GelMA confirming the functionality of the selected blend shortly after fabrication (3days) by Phalloidin (Red) / DAPI (blue) staining. Cell-Material interactions demonstrated by cell protrusions (arrows) are visible in 3D and 2D projection (scale bars 100µm). d | hASCs in suspension were also able to adhere to these 1:1 GG/GelMA fibres, fully engulfing them after 1 week of culture with the structure still retaining its shape (scale bars 100µm).

Overall, our approach allowed to screen the impact of changes in the 3D cell environment on distinct, relevant markers, trends which - as we also show - recapitulate what takes place molecularly in GG *versus* GelMA macro hydrogels (**S15, S16**). Moreover, we could not only detect said trends but also pinpoint a specific setpoint where the change from inert-like encapsulation to active cell-biomaterial interaction appears to take place. To put this to test, we fabricated uniform fibres of the 1:1 GG/GelMA blend with encapsulated and suspended hASCs. Shortly after fabrication, cell-material interactions could be already detected both within the fibre (**fig. 5c)** and also on the outer surface (**fig. 5d**), showing an immediate and successful application of the HT screening method to identify the most suitable material (composition) to maximize a specific cellular response for a certain application. On the one hand, this cell-material interaction was never observed on GG hydrogels and, on the other hand, pure GelMA structures quickly degrade and as such are not stable [33,34], yet both cell interaction and fibre stability were present in the optimized blend.

In summary, we have demonstrated how the microfluidic manipulation of hydrogel precursors can be used to fabricate 3D material gradients sequentially and with high efficiency, creating independent cell-laden libraries that can integrate different types of materials and crosslinking, obtaining both gradients purely with ionic crosslinking materials and also gradients with a switch from an ionic-crosslinking material (GG) to an UV-crosslinking one (GelMA). These gradients were in all cases fabricated as individual structures and further subjected to different culture stimuli. Cell's responses were tracked continuously along the gradient length connecting their relative position to the corresponding 3D environment composition, knowing gradients were linearly fabricated. We also validated our results by establishing a low-throughput parallel with macro, uniform hydrogels and molecular validation of microscopy and image analysis data, proving the recapitulation of the responses observed within the microfibre gradients.

Gradients with a range of GG concentration showed that hASCs' responses in non-adhesive encapsulation scenarios could be affected by softer/stiffer environments which can be optimized to better trigger the master regulators of adipogenesis /chondrogenesis, respectively (**fig. 6a**).

Conclusions

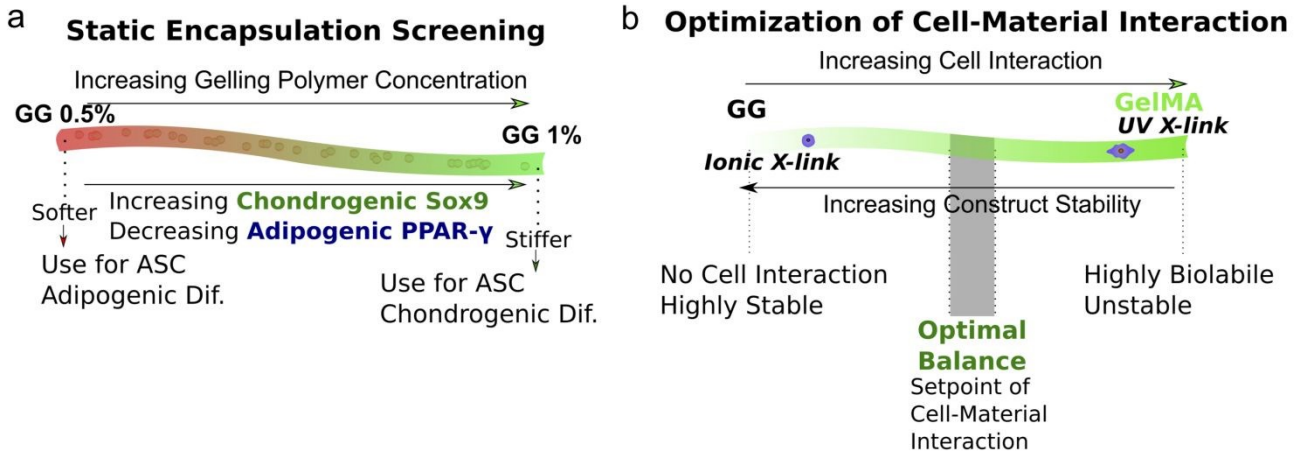

Fig. 6: High-throughput Power of 3D Gradients: Our microfluidic approach can be used to fabricate gradient libraries of concentration of a single ionic crosslinking material (a) or to optimize the combination of distinct materials and crosslinking type to test different cell responses (b). Non-adhesive material-based fibres represent suitable platforms to assess the influence of the materials' mechanical properties over stromal/stem cells under pro-differentiation culture conditions as exemplified by the stiffer GG regions that provide a better triggering of chondrogenic differentiation whereas softer ones are more prone for triggering adipogenic commitment. Moreover, non-adhesive materials might benefit from blending with more biolabile and cell-adhesive ones such as the case of the blending of GG with GelMA (b). The gradient platforms fabricated with these distinct materials allowed not only screening cell adhesion-related responses but quickly detecting a setpoint and a specific formulation at which mechanical and biological performance were maximized, advantage of having a continuous approach where all in-between conditions are considered as opposed to discrete, low-throughput alternatives.

View Article Online DOI: 10.1039/D0MH00818D

Gradients with a full switch in the composing material from ionic-crosslinkable GG to UV-crosslinkable GelMA revealed not only trends but a setpoint of cell-material interaction at around 1:1 GG/GelMA ratio, an efficient optimization of the combination of the structural stability of GG with the cell interaction properties of GelMA (**fig. 6b**).

We believe the simplicity and generality of our approach might push cell-biomaterial screening to higher throughput and globally faster discoveries as well as optimization and personalization of TERM strategies. Within the same field, it might also prove to be a powerful tool for the biofabrication of interface tissues that naturally bridge distinct mechanical and cellular environments [35]. On a broader perspective, the possibility of creating hydrogel gradients without the need of light-dependent, covalent crosslinking might also bring answers to fundamental questions focusing on distinct cellular responses to gradually-changing conditions, e.g. durotaxis [36], by introducing ionic-crosslinkable and consequently stress-relaxing environments that more closely mimic living tissue environments [18].

There is nevertheless an important gap that remains open, which is the complete combination of 3D cell/material conditions with fully 3D imaging and analysis. Currently, imaging and computational limitations make this type of analysis a significant constraint in high-throughput by demanding complex, time-consuming operations [37]. We expect, however, that recent advances in faster 3D fluorescent imaging as well as efforts towards more efficient 3D data storage and processing will provide off-the-shelf solutions and software soon. At that point, their integration with platforms as the one hereby communicated will likely break the final frontier of complete 3D HT cell/biomaterial screening.

Conflicts of interest

There are no conflicts to declare.

Acknowledgements

The authors acknowledge financial support from the European Research Council, grant ERC-2012-ADG 20120216-321266 (project ComplexiTE). C.F.G. acknowledges scholarship PD/BD/135253/2017 from Fundação para a Ciência e Tecnologia (FCT). Doctor Dillip K. Biship is kindly acknowledged for the help with confocal microscopy.

References

1 M. P. Lutolf, P. M. Gilbert and H. M. Blau, *Nature*, 2009, **462**, 433–441.
2 W. J. Hadden, J. L. Young, A. W. Holle, M. L. McFetridge, D. Y. Kim, P. Wijesinghe, H. Taylor-Weiner, J. H. Wen, A. R. Lee, K. Bieback, B.-N. Vo, D. D. Sampson, B. F. Kennedy, J. P. Spatz, A. J. Engler and Y. S. Choi, *Proc. Natl. Acad. Sci.*, 2017, **114**, 5647–5652.
3 Q. Zhou, O. Castañeda Ocampo, C. F. Guimarães, P. T. Kühn, T. G. Van Kooten and P. Van Rijn, *ACS Appl. Mater. Interfaces*, , DOI:10.1021/acsami.7b08237.
4 S. L. Vega, M. Y. Kwon, K. H. Song, C. Wang, R. L. Mauck, L. Han and J. A. Burdick, *Nat. Commun.*, 2018, **9**, 614.
5 S. Pedron, E. Becka and B. A. Harley, *Adv. Mater.*, 2015, **27**, 1567–1572.
6 L. G. Major, A. W. Holle, J. L. Young, M. S. Hepburn, K. Jeong, L. Ian, R. W. Sanderson, J. H. Jeong, Z. M. Aman, B. F. Kennedy, D. Han, H. W. Park, K. Guan, J. P. Spatz and Y. S. Choi, *ACS Appl. Mater. Interfaces*, 2019, 45520–45530.
7 L. Gasperini, A. P. Marques and R. L. Reis, Patent *WO2018078562A1, 2018*.
8 F. F. B. Hulshof, Y. Zhao, A. Vasilevich, N. R. M. Beijer, M. de Boer, B. J. Papenburg, C. van Blitterswijk, D. Stamatialis and J. de Boer, *Acta Biomater.*, 2017, **62**, 188–198.
9 D. G. Anderson, D. Putnam, E. B. Lavik, T. A. Mahmood and R. Langer, *Biomaterials*, 2005, **26**, 4892–4897.
10 H. D. Kim, E. A. Lee, Y. H. Choi, Y. H. An, R. H. Koh, S. L. Kim and N. S. Hwang, *Acta Biomater.*, 2016, **34**, 21–29.
11 O. Jeon, D. S. Alt, S. W. Linderman and E. Alsberg, *Adv. Mater.*, 2013, **25**, 6366–6372.
12 K. Chatterjee, M. F. Young and C. G. Simon, *Comb. Chem. High Throughput Screen.*, 2011, **14**, 227–236.
13 A. Lee, A. R. Hudson, D. J. Shiwarski, J. W. Tashman, T. J. Hinton, S. Yerneni, J. M. Bliley, P. G. Campbell and A. W. Feinberg, *Science (80-.).*, 2019, **365**, 482–487.
14 L. R. Stevens, K. J. Gilmore, G. G. Wallace and M. In het Panhuis, *Biomater. Sci.*, 2016.
15 C. F. Guimarães, L. Gasperini, A. P. Marques and R. L. Reis, *Nat. Rev. Mater.*, 2020, DOI:10.1038/s41578-019-0169-1.
16 T. Rada, R. L. Reis and M. E. Gomes, *Tissue Eng. - Part B Rev.*, 2009, **15**, 113–125.
17 A. F. Carvalho, L. Gasperini, R. S. Ribeiro, A. P. Marques and R. l. Reis, *J. Tissue Eng. Regen. Med.*, 2018, **12**, e1063–e1067.
18 O. Chaudhuri, L. Gu, D. Klumpers, M. Darnell, S. A. Bencherif, J. C. Weaver, N. Huebsch, H. P. Lee, E. Lippens, G. N. Duda and D. J. Mooney, *Nat. Mater.*, 2015, **15**, 326–334.
19 H. P. Lee, L. Gu, D. J. Mooney, M. E. Levenston and O. Chaudhuri, *Nat. Mater.*, 2017, **16**, 1243–1251.
20 P. Samal, P. Maurer, C. Van Blitterswijk, R. Truckenmüller and S. Giselbrecht, *Adv. Mater.*, , DOI:10.1002/adma.201907966.
21 Y. Kawakami, J. Rodriguez-León and J. C. I. Belmonte, *Curr. Opin. Cell Biol.*, 2006, **18**, 723–729.
22 T. J. Kwak, Y. G. Nam, M. A. Najera, S. W. Lee, J. R. Strickler and W. J. Chang, *PLoS One*, 2016, **11**, 1–15.
23 J. Xie, D. Zhang, C. Zhou, Q. Yuan, L. Ye and X. Zhou, *Acta Biomater.*, 2018, **79**, 83–95.
24 L. G. Major and Y. S. Choi, *J. Tissue Eng. Regen. Med.*, 2018, 1–8.
25 B. Teong, S. C. Wu, C. M. Chang, J. W. Chen, H. T. Chen, C. H. Chen, J. K. Chang and M. L. Ho, *J. Biomed. Mater. Res. - Part B Appl. Biomater.*, 2018, **106**, 808–816.
26 E. D. Rosen and O. A. MacDougald, *Nat. Rev. Mol. Cell Biol.*, 2006, **7**, 885–896.
27 M. Lago, L. da Silva, C. Henriques, A. Carvalho, R. Reis and A. Marques, *Bioengineering*, 2018, **5**, 52.
28 G. S. Hussey, J. L. Dziki and S. F. Badylak, *Nat. Rev. Mater.*, 2018, **3**, 159–173.
29 J. W. Nichol, S. T. Koshy, H. Bae, C. M. Hwang, S. Yamanlar and A. Khademhosseini, *Biomaterials*, 2010, **31**, 5536–5544.
30 E. Biela, J. Galas, B. Lee, G. L. Johnson, Z. Darzynkiewicz and J. W. Dobrucki, *Cytom. Part A*, 2013, **83 A**, 533–539.
31 S. Dupont, L. Morsut, M. Aragona, E. Enzo, S. Giulitti, M. Cordenonsi, F. Zanconato, J. Le Digabel, M. Forcato, S. Bicciato, N. Elvassore and S. Piccolo, *Nature*, 2011, **474**, 179–184.
32 H. Lee, R. Stowers and O. Chaudhuri, *Nat. Commun.*, 2019, **10**, 529.
33 M. Zhu, Y. Wang, G. Ferracci, J. Zheng, N. J. Cho and B. H. Lee, *Sci. Rep.*, 2019, **9**, 1–13.
34 Y. Fukunaka, K. Iwanaga, K. Morimoto, M. Kakemi and Y. Tabata, *J. Control. Release*, 2002, **80**, 333–343.
35 S. Ansari, S. Khorshidi and A. Karkhaneh, *Acta Biomater.*, 2019, **87**, 41–54.
36 R. Sunyer, V. Conte, J. Escribano, A. Elosegui-Artola, A. Labernadie, L. Valon, D. Navajas, J. M. García-Aznar, J. J. Muñoz, P. Roca-Cusachs and X. Trepat, *Science (80-.).*, 2016, **353**, 1157–1161.
37 T. H. Booij, L. S. Price and E. H. J. Danen, *SLAS Discov.*, 2019, **24**, 615–627.